

## Energy Transfer

## Corononetetraimide-Centered Cruciform Pentamers Containing Multiporphyrin Units: Synthesis and Sequential Photoinduced Energy- and Electron-Transfer Dynamics

Taku Hasobe,<sup>\*[a]</sup> Koichi Ida,<sup>[a]</sup> Hayato Sakai,<sup>[a]</sup> Kei Ohkubo,<sup>[b, c]</sup> and Shunichi Fukuzumi<sup>\*[b, c, d]</sup>

**Abstract:** A series of corononetetraimide (CorTIm)-centered cruciform pentamers containing multiporphyrin units, in which four porphyrin units are covalently linked to a CorTIm core through benzyl linkages, were designed and synthesized to investigate their structural, spectroscopic, and electrochemical properties as well as photoinduced electron- and energy-transfer dynamics. These systems afforded the first synthetic case of coroneneimide derivatives covalently linked with dye molecules. The steady-state absorption and electrochemical results indicate that a CorTIm and four porphyrin units were successfully characterized by the corresponding reference monomers. In contrast, the steady-state fluorescence measurements demonstrated that strong fluorescence quenching relative to the corresponding monomer units was observed in these pentamers. Nanosecond laser flash photolysis measurements revealed the occurrence of

intermolecular electron transfer from triplet excited state of zinc porphyrins to CorTIm. Femtosecond laser-induced transient absorption measurements for excitation of the CorTIm unit clearly demonstrate the sequential photoinduced energy and electron transfer between CorTIm and porphyrins, that is, occurrence of the initial energy transfer from CorTIm (energy donor) to porphyrins (energy acceptor) and subsequent electron transfer from porphyrins (electron donor) to CorTIm (electron acceptor) in these pentamers, whereas only the electron-transfer process from porphyrins to CorTIm was observed when we mainly excite porphyrin units. Finally, construction of high-order supramolecular patterning of these pentamers was performed by utilizing self-assembly and physical dewetting during the evaporation of solvent.

## Introduction

Disk-shaped molecules such as polycyclic aromatic hydrocarbons (PAHs) and their derivatives are finding increasing interest among other self-assembled molecular systems because of their tendency to form extended  $\pi$ -stacked assemblies.<sup>[1]</sup> Because of many potential properties such as a high electron density, these molecules are of fundamental importance not

only as models for the study of energy and electron transfer in organized systems,<sup>[2]</sup> but also as functional materials for device applications such as light-emitting diodes (LED),<sup>[3]</sup> photovoltaic cells,<sup>[2],4)</sup> and field-effect transistors (FET).<sup>[5]</sup>

In contrast to the comparatively large collection of available disk-shaped electron-donating molecules, disk-shaped electron-accepting molecular systems are still considerably underdeveloped. Fullerenes possess three-dimensional and spherical  $\pi$ -systems,<sup>[6]</sup> whereas the representative two-dimensional molecules are mainly peryleneimides (PDIs). PDIs exhibit reversible and successive first and second one-electron reduction. Therefore, PDIs are widely utilized as good electron acceptors in reaction center models for artificial photosynthesis<sup>[2b-f, h, 7]</sup> and electronic devices.<sup>[5f, 8]</sup>

On the other hand, a systematic and rational synthesis of coroneneimide derivatives has been recently reported.<sup>[9]</sup> Actually, the chemical structures of coronenes increased a great diversity of synthetic strategies for coroneneimide derivatives. For example, in the case of corononetetraimide (CorTIm), four maleimides can be fused to a coronene skeleton, whereas PDIs have only two maleimides. Consequently, the photophysical and redox properties can be systematically controlled by the type and number of substituents.<sup>[9d]</sup> In particular, CorTIm shows four reversible one-electron reduction waves because the LUMO is energetically low-lying and doubly degenerate.<sup>[9d]</sup> This is in sharp contrast with the above-mentioned trend of

[a] Prof. T. Hasobe, K. Ida, Dr. H. Sakai  
Department of Chemistry  
Faculty of Science and Technology, Keio University  
3-14-1 Hiyoshi, Yokohama, Kanagawa 223-8522 (Japan)  
E-mail: hasobe@chem.keio.ac.jp

[b] Prof. K. Ohkubo, Prof. S. Fukuzumi  
Department of Material and Life Science  
Graduate School of Engineering, Osaka University  
ALCA and SENTAN, Japan Science and Technology Agency (JST)  
Suita, Osaka, 565-0871 (Japan)  
E-mail: fukuzumi@chem.eng.osaka-u.ac.jp

[c] Prof. K. Ohkubo, Prof. S. Fukuzumi  
Department of Bioinspired Chemistry  
Ewha Womans University, Seoul 120-750 (Korea)

[d] Prof. S. Fukuzumi  
Faculty of Science and Engineering, ALCA and SENTAN  
Japan Science and Technology Agency (JST)  
Meijo University, Nagoya, Aichi 468-0073 (Japan)

Supporting information for this article is available on the WWW under <http://dx.doi.org/10.1002/chem.201500766>.

PDIs, which accept only two electrons. However, the synthesis of covalently linked donor–acceptor systems composed of coroneneimide derivatives have yet to be explored because of synthetic difficulty.

Porphyrins possess an extensively two-dimensional  $\pi$ -conjugation and basically act as electron donors<sup>[2h,6a,c,e,g,10]</sup> or energy acceptors,<sup>[11]</sup> but not electron acceptors because of the low one-electron reduction potentials (i.e., high energy level of LUMO). Therefore, synthetic covalent systems from molecular dyads and triads<sup>[2e,6b,12]</sup> to macromolecules such as oligomers<sup>[11d,13]</sup> and dendrimers<sup>[10,14]</sup> have been extensively reported to investigate sequential energy and electron transfer. Moreover, in a combination of coronenetetraimide (CorTIm) and porphyrin units, an overlap between energy donor emission (CorTIm) and acceptor absorption (porphyrin) is expected to occur in the spectral range from about 500 to 600 nm.<sup>[9d]</sup> In contrast, considering the reported first one-electron reduction potential of coronenetetraimides ( $-0.65$  V vs. SCE)<sup>[9d]</sup> and oxidation potential of zinc porphyrins ( $\approx 0.8$  V vs. SCE),<sup>[15]</sup> the energy level of the charge-separated state composed of CorTIm radical anion and porphyrin radical cation is approximately estimated to be  $\approx 1.5$  eV, which is smaller than the single and triplet excited energies of these molecules. Thus, a combination of these two units seems ideal for enhancing the light-harvesting efficiency and the resulting energy and electron transfer throughout the solar spectrum.

On the basis of the above consideration, we newly synthesized new coronenetetraimide (energy donor and electron acceptor)-centered cruciform pentamers containing four porphyrins (energy acceptor and electron donor) as shown in Figure 1. In this study, we report the details of the synthesis as well as spectroscopic and photophysical properties of these molecules including the sequential energy and electron transfer.

## Results and Discussion

### Synthesis

To achieve synthesis of cruciform pentamer,  $(\text{H}_2\text{P})_4\text{-CorTIm}$ , a synthetic scheme of maleimidation of coroneneimide was proposed on the basis of the maleimidation of coroneneoctacarboxylic acid derived from  $\text{CorDIm}(\text{iBu})_4$  and porphyrin **5** (Scheme 1). Here it should be noted that direct introduction of 4-aminomethyl-phenyl group onto a porphyrin ring from monobromo-substituted porphyrin by Suzuki–Miyaura coupling did not proceed. Therefore, we employed a synthetic strategy to protect the  $\text{NH}_2$  unit as a phthalimide as shown in Scheme 1. In particular, the coupling reaction between monobromo-substituted freebase porphyrin and aryl boronic acid did not proceed well. Therefore, we employed zinc porphyrin derivatives in the initial step and then removed the zinc from the porphyrin center to perform the subsequent reactions.

On the basis of on the above considerations, first, bromination of porphyrin **1** was carried out with NBS at  $0^\circ\text{C}$  for synthesis of porphyrin **2**.<sup>[16]</sup> Next, porphyrin **3** was synthesized by Suzuki–Miyaura coupling of porphyrin **2** and aryl boronic acid.<sup>[17]</sup> To remove the zinc unit, porphyrin **3** was treated with

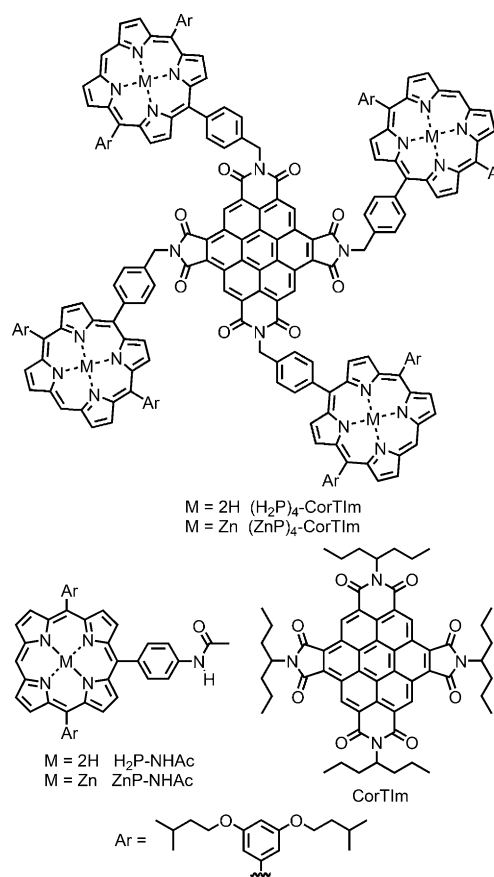


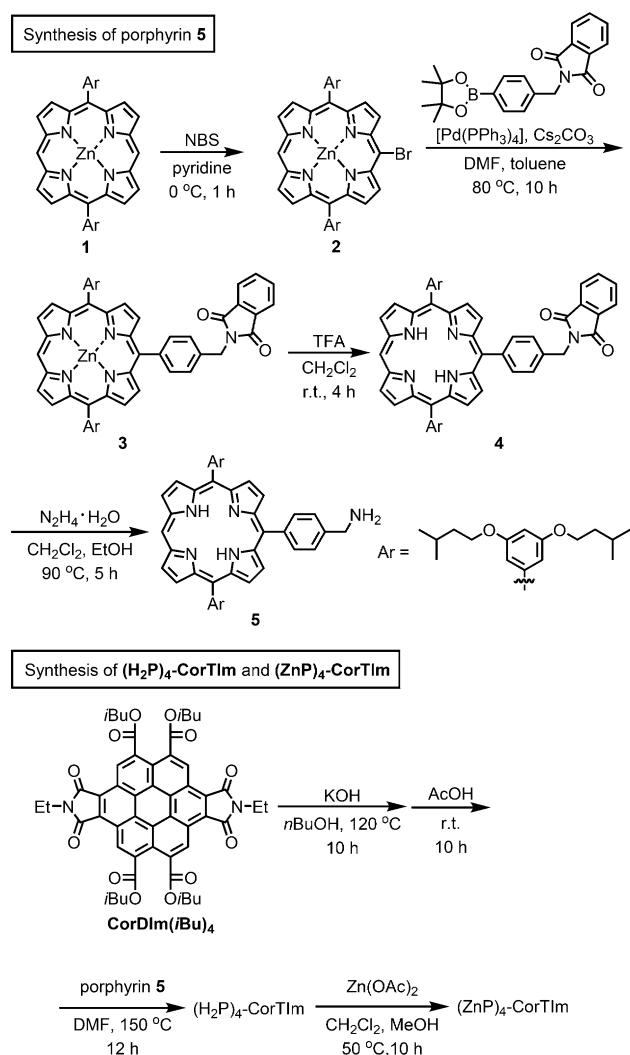
**Figure 1.** Chemical structures of donor–acceptor cruciform pentamers  $(\text{H}_2\text{P})_4\text{-CorTIm}$  and  $(\text{ZnP})_4\text{-CorTIm}$  and reference compounds employed in this work.

trifluoroacetic acid (TFA) to obtain the free base porphyrin **4**. Then, porphyrin **5**, which is a precursor of  $(\text{H}_2\text{P})_4\text{-CorTIm}$ , was obtained by replacing the phthalimide of porphyrin **4** with an amino group under basic conditions.

With regard to the synthesis of coroneneoctacarboxylic acid, which is a precursor of  $(\text{H}_2\text{P})_4\text{-CorTIm}$ , first, the isobutoxycarbonyl groups of  $\text{CorDIm}(\text{iBu})_4$  were replaced with a carboxylate anion under basic conditions.<sup>[9a]</sup> To synthesize coroneneoctacarboxylic acid, protonation of carboxylate anion was carried out by using acetic acid, which was followed by dehydration under vacuum. Because of accomplished preparation of each precursor for the synthesis of  $(\text{H}_2\text{P})_4\text{-CorTIm}$ ,  $(\text{H}_2\text{P})_4\text{-CorTIm}$  was synthesized by dehydration condensation of each precursor. The synthesized pentamer was characterized by the  $^1\text{H}$  NMR and  $^{13}\text{C}$  NMR spectroscopy and MALDI-TOF MS (see the Experimental Section and Figure S1 in the Supporting Information). The synthesis of  $(\text{ZnP})_4\text{-CorTIm}$  was finally achieved by the insertion of zinc into the center of the free base porphyrin macrocycle.

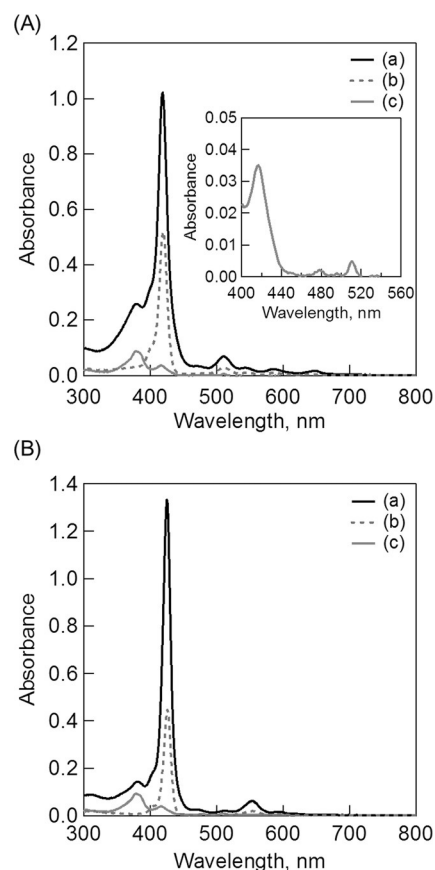
### Steady-state absorption spectra

Figure 2 displays the absorption spectra of  $(\text{H}_2\text{P})_4\text{-CorTIm}$  (Figure 2A) and  $(\text{ZnP})_4\text{-CorTIm}$  (Figure 2B) in benzonitrile (PhCN).



**Scheme 1.** Synthetic schemes of porphyrin 5,  $(\text{H}_2\text{P})_4\text{-CorTIm}$ , and  $(\text{ZnP})_4\text{-CorTIm}$ .

By comparing the spectra of  $(\text{H}_2\text{P})_4\text{-CorTIm}$  and  $(\text{ZnP})_4\text{-CorTIm}$  with those of the corresponding reference monomer compounds, we can identify the respective peaks of porphyrin and CorTIm units. For example, in  $(\text{H}_2\text{P})_4\text{-CorTIm}$  (spectrum a in Figure 2A), a CorTIm unit has an absorption maximum at 380 nm, whereas an intense Soret band at 419 nm and four Q-bands at 511, 544, 586, and 648 nm were observed in porphyrin units, which are derived from the typical spectral features in free base porphyrin monomer (spectra b and c in Figure 2A). More importantly, the absorption maxima of  $(\text{H}_2\text{P})_4\text{-CorTIm}$  are the same as those of the respective reference compounds ( $\text{H}_2\text{P-NHAc}$  and CorTIm) as shown in spectra b and c in Figure 2A. As a consequence, we can conclude that a CorTIm and four porphyrin units in  $(\text{H}_2\text{P})_4\text{-CorTIm}$  were basically characterized by the corresponding monomers, although the broadened feature was slightly observed in the Soret and Q-bands. These trends were also similarly observed for  $(\text{ZnP})_4\text{-CorTIm}$  in Figure 2B, which exhibits an absorption maximum of CorTIm unit at 381 nm, an intense Soret band at 425 nm, and three Q-bands at 513, 550, and 594 nm.



**Figure 2.** Steady-state absorption spectra of (A) (a)  $(\text{H}_2\text{P})_4\text{-CorTIm}$  (—), (b)  $\text{H}_2\text{P-NHAc}$  (----), and (c) CorTIm (—) in PhCN; (B) (a)  $(\text{ZnP})_4\text{-CorTIm}$  (—), (b)  $\text{ZnP-NHAc}$  (----), and (c) CorTIm (—) in PhCN. The concentrations were  $1.0 \mu\text{M}$  in all systems. The inset of (A) shows the enlarged spectrum of CorTIm in the long wavelength region for clarification.

### Steady-state fluorescence spectra

Steady-state fluorescence spectra of  $(\text{H}_2\text{P})_4\text{-CorTIm}$  and reference molecules (i.e.,  $\text{H}_2\text{P-NHAc}$  and CorTIm) with the excitation at 585 and 380 nm are shown in Figure 3A and 3B, respectively. These excitation wavelengths mainly correspond to absorption maxima of Q-band in porphyrin unit (585 nm) and CorTIm unit (380 nm) (Figure 2A). Then, we fixed the same absorbance for excitation wavelength at 585 or 380 nm to compare the quenching efficiencies between  $(\text{H}_2\text{P})_4\text{-CorTIm}$  and  $\text{H}_2\text{P-NHAc}$ . The fluorescence spectrum of  $\text{H}_2\text{P-NHAc}$  with excitation at 585 nm (spectrum a in Figure 3A) shows only two peaks at 645 and 709 nm, which are assigned to the emission from the porphyrin unit. In contrast, the emission of  $(\text{H}_2\text{P})_4\text{-CorTIm}$  was strongly quenched ( $>99\%$ ; see spectrum b in Figure 3A). These results suggest additional deactivation pathways for the excited state of the porphyrin units arising from the interaction between CorTIm<sub>4</sub> and porphyrin units in  $(\text{H}_2\text{P})_4\text{-CorTIm}$ . This may result from photoinduced electron transfer from the singlet excited state of porphyrin to CorTIm (see below). A similar trend was also observed in  $(\text{ZnP})_4\text{-CorTIm}$  (see Figure S2 in the Supporting Information).

The spectrum a in Figure 3B exhibits strong fluorescence emission bands of CorTIm at 513, 550, and 594 nm because

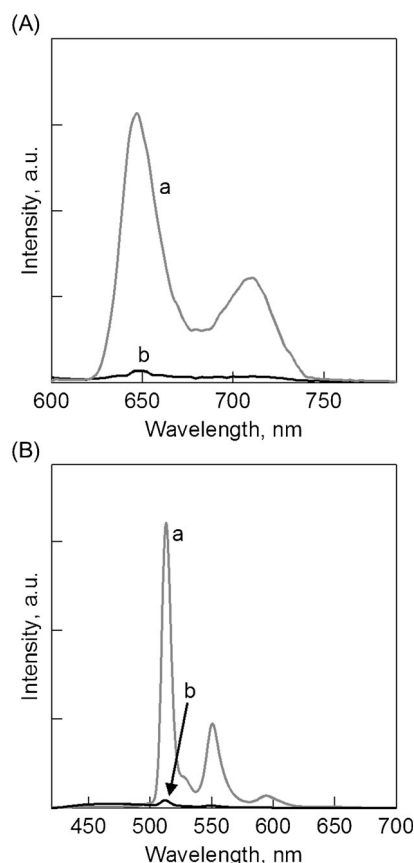


**Figure 3.** Steady-state fluorescence spectra of (A) (a)  $\text{H}_2\text{P-NHAc}$  and (b)  $0.25 \mu\text{M}$   $(\text{H}_2\text{P})_4\text{-CorTIm}$  in  $\text{PhCN}$ :  $\lambda_{\text{ex}} = 585 \text{ nm}$  and (B) (a)  $\text{CorTIm}$  and (b)  $1.0 \mu\text{M}$   $(\text{H}_2\text{P})_4\text{-CorTIm}$  in  $\text{PhCN}$ :  $\lambda_{\text{ex}} = 380 \text{ nm}$ .

the absorption band of  $\text{CorTIm}$  unit is excited. The fluorescence of  $(\text{H}_2\text{P})_4\text{-CorTIm}$  is significantly quenched compared with that of  $\text{CorTIm}$  (spectrum b in Figure 3B). The possible reason is occurrence of energy transfer from  $\text{CorTIm}$  to porphyrins because of large overlap between emission bands of  $\text{CorTIm}$  and absorption bands (Q-bands) of the porphyrins at around about 500–600 nm region (see above). However, the emission bands derived from the porphyrins were not clear because photoinduced electron transfer may occur through the singlet excited states of porphyrins after energy transfer from  $\text{CorTIm}$  to porphyrins. To carefully check the photodynamics, the excitation spectrum of  $(\text{H}_2\text{P})_4\text{-CorTIm}$  was measured (Figure S3 in the Supporting Information). The observed wavelength was 650 nm, which corresponds to the emission band of porphyrins. Although the signal-to-noise ratio (S/N) is not low because of the occurrence of efficient photoinduced electron transfer, the excitation spectrum roughly agrees with the corresponding absorption spectrum of  $(\text{H}_2\text{P})_4\text{-CorTIm}$  with an absorption peak at about 380 nm (Figure S3 in the Supporting Information). On the basis of these results, we suggest that the initial energy transfer from the singlet excited state of  $\text{CorTIm}$  to porphyrins and subsequent electron transfer from the porphyrin to  $\text{CorTIm}$  occur when  $\text{CorTIm}$  is mainly excited. Additionally, femtosecond time-resolved transient absorption measurements strongly support the above discussion (see below). A

similar trend was also observed in the case of  $\text{ZnP-NHAc}$  and  $(\text{ZnP})_4\text{-CorTIm}$  (Figure S2 in the Supporting Information).

### Electrochemical measurements

We next performed electrochemical measurements by using cyclic voltammetry to determine the first one-electron reduction and oxidation potentials of these pentamers. In these measurements, we employed  $\text{CH}_2\text{Cl}_2$  as a solvent because of the limited solubility. Figure 4 shows the cyclic voltammograms of  $(\text{ZnP})_4\text{-CorTIm}$  and the reference compounds in  $\text{CH}_2\text{Cl}_2$ . The summarized electrochemical data are shown in Table 1.  $(\text{ZnP})_4\text{-}$

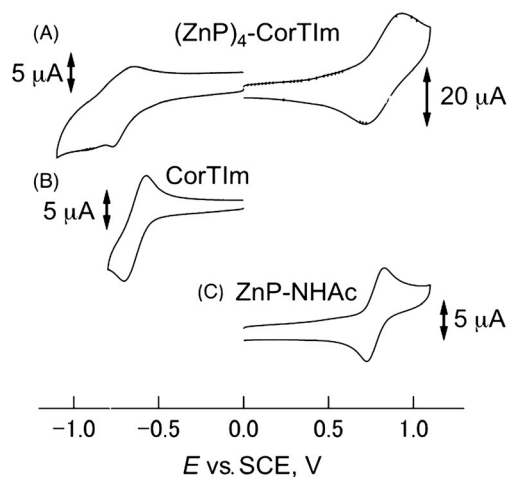


**Figure 4.** Cyclic voltammograms of (A)  $(\text{ZnP})_4\text{-CorTIm}$ ; (B)  $\text{CorTIm}$ ; and (C)  $\text{ZnP-NHAc}$  in  $\text{CH}_2\text{Cl}_2$  with  $0.3 \text{ M } n\text{-Bu}_4\text{NPF}_6$  as the supporting electrolyte. Scan rate:  $200 \text{ mV s}^{-1}$ .

**Table 1.** First one-electron reduction and oxidation potentials of  $(\text{H}_2\text{P})_4\text{-CorTIm}$ ,  $(\text{ZnP})_4\text{-CorTIm}$ , and the reference compounds.

Compounds	$E_{\text{red}}$ , V vs. SCE <sup>[a]</sup> [V]	$E_{\text{ox}}$ , V vs. SCE <sup>[a]</sup> [V]
$(\text{ZnP})_4\text{-CorTIm}$	−0.72	+0.83
$(\text{H}_2\text{P})_4\text{-CorTIm}$	−0.72	+1.00
$\text{CorTIm}$	−0.65	–
$\text{ZnP-NHAc}$	−1.41	+0.78
$\text{H}_2\text{P-NHAc}$	−1.26	+0.95

[a] Measured in  $\text{CH}_2\text{Cl}_2$  containing  $0.3 \text{ M } n\text{-Bu}_4\text{NPF}_6$  at 298 K.

$\text{CorTIm}$  exhibits reversible redox waves, which are typical for the first one-electron oxidation ( $\text{ZnP}^+/\text{ZnP}$ ) and reduction processes ( $\text{CorTIm}/\text{CorTIm}^-$ ). The first one-electron reduction ( $E_{\text{red}}$ ) and oxidation ( $E_{\text{ox}}$ ) potentials were assigned to be −0.72 and 0.83 V versus SCE, respectively (Figure 4A). These values are very similar to those of reference single components such as  $E_{\text{red}}$  of  $\text{CorTIm}$ : −0.65 V and  $E_{\text{ox}}$  of  $\text{ZnP-NHAc}$ : 0.78 V as shown in Figure 4B and 4C. The electrochemical results indicate that a  $\text{CorTIm}$  and four porphyrin units in  $(\text{H}_2\text{P})_4\text{-CorTIm}$  were characterized by the corresponding reference monomers in solution, which is similar to the trend of absorption spectra in

Figure 2. Considering the above electrochemical data, the energy level of the charge-separated state of CorTIm and ZnP unit (i.e., CorTIm radical anion and ZnP radical cation) was determined from the difference between  $E_{ox}$  of ZnP and  $E_{red}$  of CorTIm in  $(ZnP)_4$ -CorTIm to be 1.55 eV. This value is smaller than the excited energies of each chromophore: 2.08 and 1.59 eV for the singlet and triplet excited states of zinc porphyrins<sup>[15]</sup> and 2.42 and 2.02 eV for the singlet and triplet excited states of CorTIm,<sup>[9d]</sup> respectively (see later; Figure 7).

### Intermolecular photoinduced electron transfer monitored by nanosecond laser flash photolysis

To discuss the electron-accepting properties of pristine CorTIm, nanosecond laser flash photolysis measurements were performed to examine intermolecular electron transfer from the triplet excited state of ZnP-NHAc to CorTIm in PhCN (Figure 5). The excitation wavelength was chosen as 532 nm to excite porphyrins. We can clearly observe relatively strong radical anion bands of CorTIm ( $CorTIm^{\cdot-}$ ) at around the 500–700 nm and 800–950 nm regions upon laser pulse excitation, whereas the corresponding broad bands of porphyrin radical

cation were seen at around the 600–750 nm region (Figure 5A).<sup>[15]</sup> The absorption spectrum of  $CorTIm^{\cdot-}$  is also shown in Figure S4 (the Supporting Information). The decay of the transient absorption at 930 nm due to  $CorTIm^{\cdot-}$  obeyed second-order kinetics, indicating that the charge-recombination by back electron transfer (BET) occurred through a bimolecular process (Figure 5B). From the slope of the plot in the inset of Figure 5B, the second-order rate constant was determined to be  $5.5 \times 10^9 \text{ M}^{-1} \text{ s}^{-1}$ , which is very close to the diffusion-limited value in PhCN.<sup>[18]</sup> This is in sharp contrast with the intramolecular electron transfer through singlet excited states in  $(ZnP)_4$ -CorTIm (see below). It should be noted that no transient signals were observed within the time resolution of nanosecond transient measurements in both  $(H_2P)_4$ -CorTIm and  $(ZnP)_4$ -CorTIm. Therefore, femtosecond laser flash photolysis measurements were performed to examine the much faster process as discussed in the next section.

### Ultrafast intramolecular photoinduced processes monitored by femtosecond laser-induced transient absorption

Time-resolved transient absorption spectra of  $(ZnP)_4$ -CorTIm and  $(H_2P)_4$ -CorTIm in PhCN were measured by femtosecond laser photolysis. The transient absorption spectra of pristine porphyrin (ZnP-NHAc), CorTIm,  $(ZnP)_4$ -CorTIm, and  $(H_2P)_4$ -CorTIm in deaerated PhCN were also measured by using a 430 nm femtosecond laser pulse (fwhm = 130 fs), which selectively excited only the porphyrin units. Figure 6A and 6B show the transient absorption spectra of the reference ZnP-NHAc and CorTIm single components to assign the singlet-singlet transient absorption bands, respectively. The transient spectrum of  $H_2P$ -NHAc is shown in Figure S5 (the Supporting Information) for comparison. In both cases, broad transient absorption bands at around the 400–800 nm for ZnP-NHAc and the 600–800 nm region for CorTIm were observed.

Figures 6C and 6D also show the transient absorption spectra of  $(ZnP)_4$ -CorTIm and  $(H_2P)_4$ -CorTIm in PhCN, respectively. Two strong transient absorption bands immediately appeared after laser-pulse excitation. The absorption band at 500–700 nm is probably attributable to the overlapped components of the singlet-singlet absorption of porphyrins and the radical cation of porphyrins.<sup>[15]</sup> The other band at about 860 nm is ascribed to the  $CorTIm/CorTIm^{\cdot-}$  (see Figure S6 in the Supporting Information). It should be noted that  $\lambda_{max}$  of  $CorTIm^{\cdot-}$  unit in  $(ZnP)_4$ -CorTIm at 862 nm is blueshifted compared with that of pristine  $CorTIm^{\cdot-}$  (922 nm).

These values of radical anions were carefully confirmed by spectroelectrochemical measurements under a negative applied voltage (see Figures S4 and S6 in the Supporting Information).<sup>[19]</sup> In this case, direct charge separation occurred after photoexcitation as discussed above, because the porphyrin moieties were directly excited. The lifetimes for the charge-recombination were approximately assigned to be 82 ps for  $(ZnP)_4$ -CorTIm and 210 ps for  $(H_2P)_4$ -CorTIm, respectively.

Figures 6E and 6F also demonstrate the transient absorption spectra of  $(ZnP)_4$ -CorTIm and  $(H_2P)_4$ -CorTIm with 393 nm laser excitation. The emphasis is that we mainly excited CorTIm

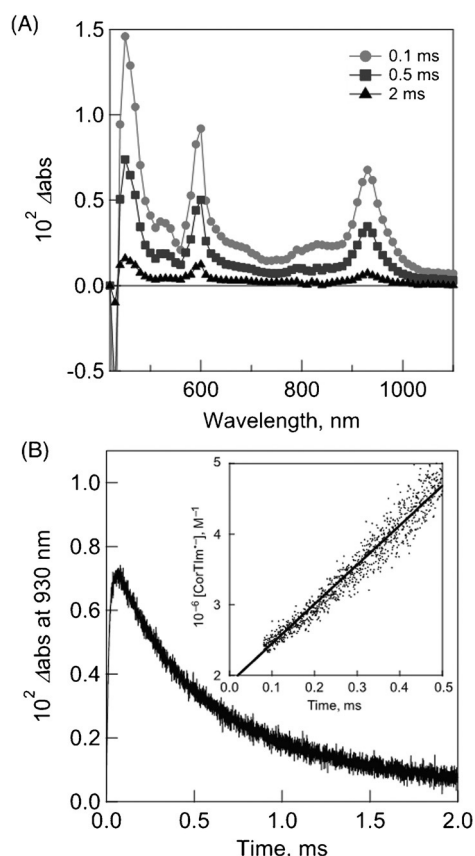


**Figure 5.** (A) Nanosecond transient absorption spectra of ZnP-NHAc (30  $\mu\text{M}$ ) with CorTIm (60  $\mu\text{M}$ ) in deaerated PhCN taken at 0.1 ms (●), 0.5 ms (■), and 2.0 ms (▲) after laser excitation at 532 nm; (B) The time profile of absorbance at 930 nm due to the  $CorTIm^{\cdot-}$ . The inset Figure shows second-order plot for decay of  $CorTIm^{\cdot-}$ .  $[CorTIm^{\cdot-}]$  is obtained from the absorbance at 930 nm and molar absorption coefficient value  $\epsilon$  of  $13500 \text{ M}^{-1} \text{ cm}^{-1}$  (see: Figure S4 in the Supporting Information).

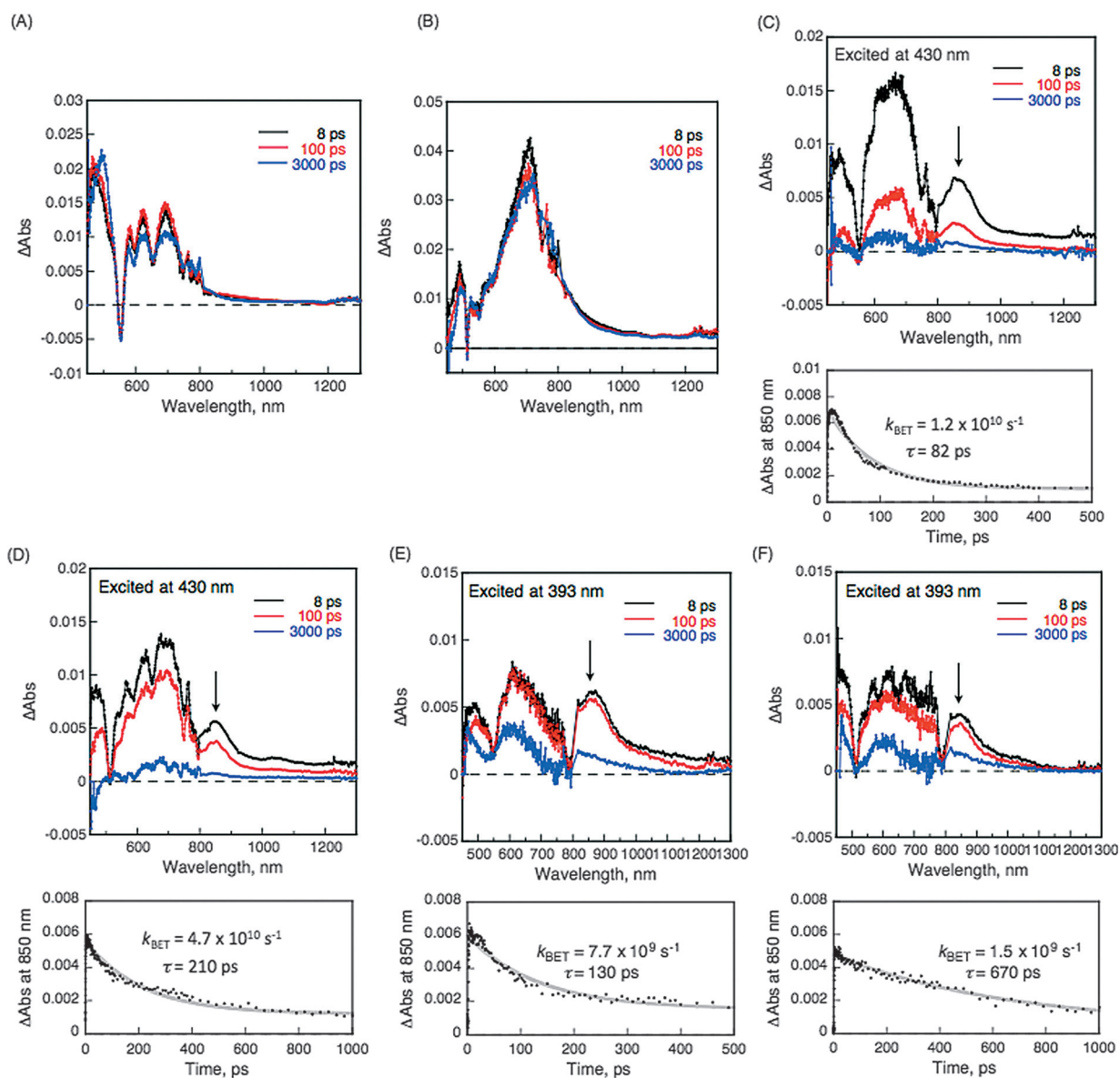


**Figure 6.** Femtosecond transient absorption spectra and corresponding time profiles of (A) 5.0  $\mu\text{M}$  ZnP–NHAc (excited at 430 nm); (B) 30  $\mu\text{M}$  CorTIm (excited at 430 nm); (C) 5.0  $\mu\text{M}$  (ZnP)<sub>4</sub>–CorTIm (excited at 430 nm); (D) 5.0  $\mu\text{M}$  (H<sub>2</sub>P)<sub>4</sub>–CorTIm (excited at 430 nm); (E) 30  $\mu\text{M}$  (ZnP)<sub>4</sub>–CorTIm (excited at 393 nm); and (F) 30  $\mu\text{M}$  (H<sub>2</sub>P)<sub>4</sub>–CorTIm (excited at 393 nm) in PhCN.

units. Judging from the above-mentioned absorption spectrum of (ZnP)<sub>4</sub>–CorTIm (Figure 2B), approximately 70 and 50% of absorption at 380 and 393 nm are attributable to the CorTIm unit in (ZnP)<sub>4</sub>–CorTIm. In addition, the lifetime of singlet excited state of CorTIm is long enough to perform photoinduced events (e.g., fluorescence lifetime  $\tau_{\text{FL}}$ : 21 ns) according to our previous work.<sup>[9d]</sup> After laser-pulse excitation of 393 nm, two transient bands at about 500–700 nm (i.e., singlet–singlet transient absorption of porphyrins and porphyrin radical cation) and about 860 nm (i.e., CorTIm radical anion) were immediately observed without a singlet–singlet absorption maximum of CorTIm at about 700 nm (Figure 6B). This clearly indicates that ultrafast energy transfer occurs from CorTIm to porphyrin units in both (ZnP)<sub>4</sub>–CorTIm and (H<sub>2</sub>P)<sub>4</sub>–CorTIm. This result also supported the above-mentioned energy-transfer from CorTIm to

porphyrins (see above). Consequently, when we mainly excite the CorTIm unit, initial energy transfer from CorTIm (energy donor) to porphyrins (energy acceptor) within several picoseconds and subsequent fast electron transfer from porphyrins (electron donor) to CorTIm (electron acceptor) occurs in these pentamers. The CS lifetimes of (ZnP)<sub>4</sub>–CorTIm and (H<sub>2</sub>P)<sub>4</sub>–CorTIm were estimated to be 130 and 670 ps, respectively. These values are much longer than those measured by excitation wavelength at 430 nm (82 ps for (ZnP)<sub>4</sub>–CorTIm and 210 ps for (H<sub>2</sub>P)<sub>4</sub>–CorTIm) because of the occurrence of the initial energy-transfer process. The energy diagram and photodynamics of (ZnP)<sub>4</sub>–CorTIm are summarized in Figure 7.

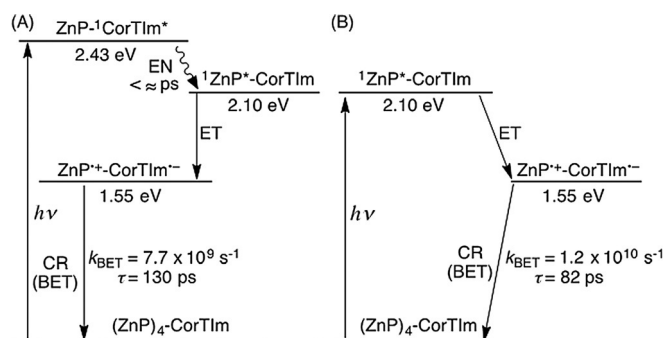


**Figure 7.** Energy diagram and photodynamics of  $(\text{ZnP})_4\text{-CorTIm}$  based on the excitation of (A) CorTIm unit and (B) ZnP unit. EN: energy transfer, ET: electron transfer and CR: charge recombination.

### High-order supramolecular patterning of $(\text{ZnP})_4\text{-CorTIm}$ observed by an atomic force microscope (AFM)

Finally, construction of high-order supramolecular structures of these pentamers was performed by utilizing self-assembly and physical dewetting during the evaporation of solvent.<sup>[20]</sup> First, we optimized the experimental conditions ( $(\text{ZnP})_4\text{-CorTIm}$  (20  $\mu\text{M}$ ) in toluene) by examining the concentration effects (10–50  $\mu\text{M}$ ) on the aggregate structures. Then, the solution (the optimized concentration: 20  $\mu\text{M}$ ) was simply cast onto the TEM grid and dried in air. In the evaporation process of solvent, the molecular pattern was effectively formed. The reference assemblies of ZnP–NHAc and CorTIm were also prepared in the same manner. Transmission electron microscope (TEM) measurements of reference ZnP–NHAc and CorTIm assemblies showed spherical and flake assemblies, respectively (Figure S7 in the Supporting Information), whereas aligned fibrous patterns were observed for  $(\text{ZnP})_4\text{-CorTIm}$  in Figure 8A. The approximate average width of  $(\text{ZnP})_4\text{-CorTIm}$  assemblies was estimated to be about 600–900 nm. The AFM measurements including the cross-sectional height information were also performed as shown in Figure 8A. The cross-sectional data showed the average height: about 20–30 nm. Considering the chemical structure of  $(\text{ZnP})_4\text{-CorTIm}$  (approximate molecular size:  $\approx 40$  Å estimated by DFT calculation) in Scheme 2, the average height approximately corresponds to approximately several layers of  $(\text{ZnP})_4\text{-CorTIm}$ -stacked assemblies.

To analyze the internal structures of  $(\text{ZnP})_4\text{-CorTIm}$  supramolecular patterning, an X-ray diffraction (XRD) measurement was performed. Although the S/N ratio is low because of the thin film, the characteristic patterns derived from two diffuse reflections were observed in the wide-angle region. The broad one centered at  $\approx 4.2$  Å corresponds to the aliphatic chains and the relatively sharper one at higher  $2\theta$  value ( $\approx 3.2$  Å) is attributable to the separation between neighboring CorTIm cores along the stacking direction.<sup>[9a,21]</sup>

To further perform absorption spectral measurements of the  $(\text{ZnP})_4\text{-CorTIm}$  assemblies,  $(\text{ZnP})_4\text{-CorTIm}$  toluene solution was cast onto a quartz plate. A similar patterning formation was successfully formed on the plate. Figure 8C shows the absorption spectra of the  $(\text{ZnP})_4\text{-CorTIm}$  assembly and the corresponding monomer in PhCN, respectively. The Soret band of

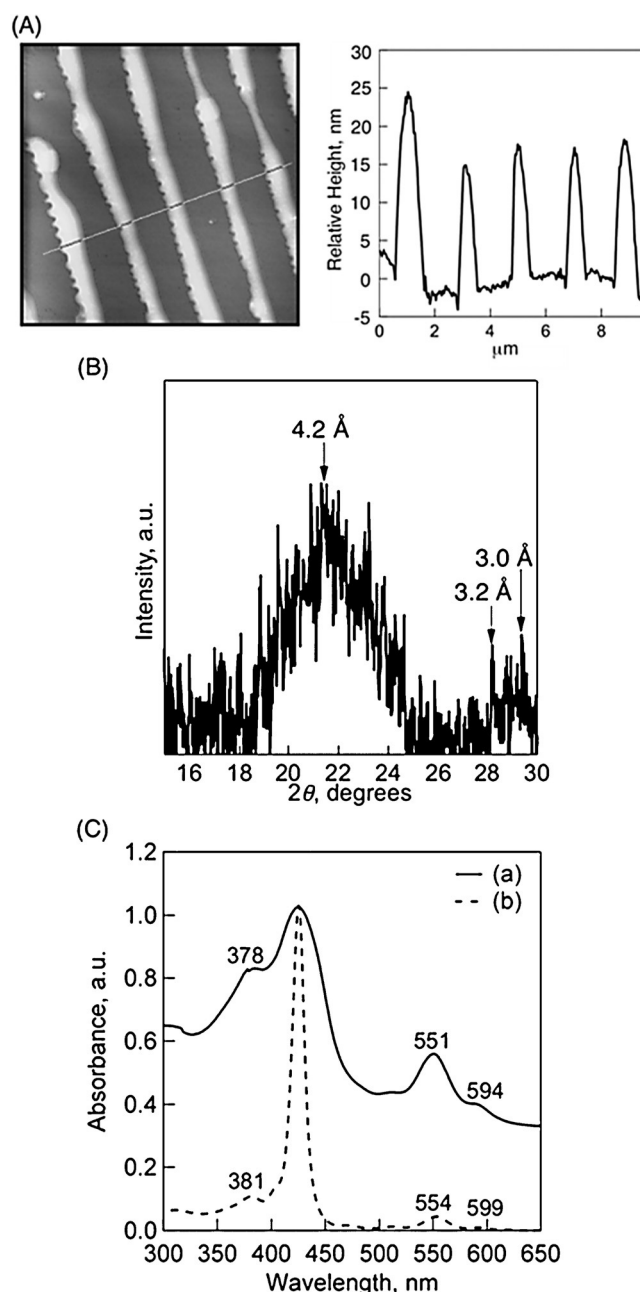
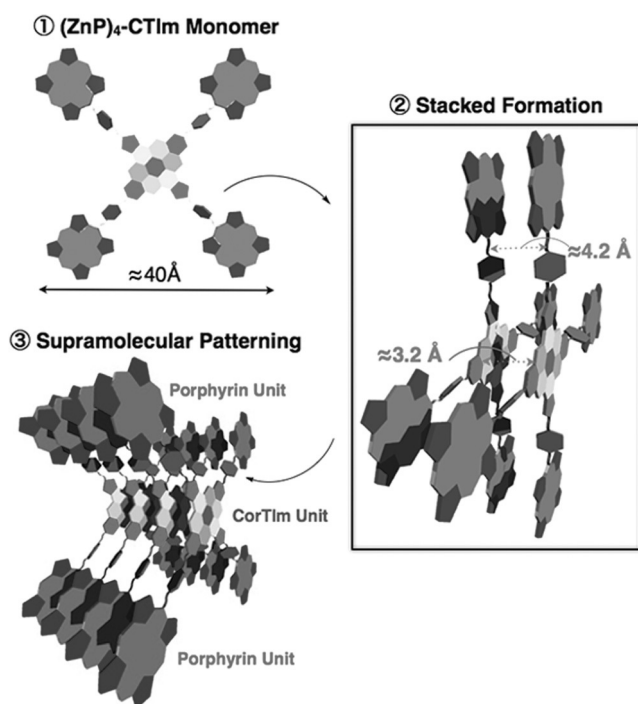


**Figure 8.** (A) AFM images of  $(\text{ZnP})_4\text{-CorTIm}$  and the corresponding cross-sectional height information. The images were taken by drop cast of the toluene solution of  $(\text{ZnP})_4\text{-CorTIm}$  onto the grid; (B) X-ray diffraction (XRD) data of  $(\text{ZnP})_4\text{-CorTIm}$ -stacked assemblies; (C) Absorption spectra of (a)  $(\text{ZnP})_4\text{-CorTIm}$ -stacked assemblies and (b)  $(\text{ZnP})_4\text{-CorTIm}$  (monomer) in PhCN.

porphyrins in  $(\text{ZnP})_4\text{-CorTIm}$  assembly became significantly broadened compared with that of the monomer solution. This clearly indicates the effective stacking alignment of neighboring porphyrin moieties based on the  $\pi\text{-}\pi$  interaction. In contrast, the band of CorTIm unit in  $(\text{ZnP})_4\text{-CorTIm}$  assembly (378 nm) became blueshifted, which suggests the columnar stacked-formation.<sup>[13a]</sup> Thus, on the basis of the above results, we can summarize the proposed internal structures of  $(\text{ZnP})_4\text{-CorTIm}$  supramolecular patterning in Scheme 2.



**Scheme 2.** A schematic illustration of proposed supramolecular structures of  $(\text{ZnP})_4\text{-CorTIm}$  and the supramolecular patterning.

## Conclusion

This work has demonstrated the synthesis and ultrafast photo-induced dynamics of coronene-tetraimide-centered cruciform pentamers containing multiporphyrin units, which are the first synthetic case of coroneneimide derivatives covalently linked with dye molecules. The spectral overlap between energy donor emission (CorTIm) and acceptor absorption (porphyrin) enabled initial ultrafast energy transfer from CorTIm (energy donor) to porphyrin (energy acceptor) units to occur within several picoseconds. Then, the appropriate redox potential gradient in these D–A units result in the occurrence of subsequent electron transfer from porphyrins (electron donor) to CorTIm (electron acceptor) in these pentamers. These processes were clearly confirmed by steady state and femtosecond time-resolved spectroscopic measurements. On the other hand, in the longer timescale, nanosecond laser flash photolysis measurements revealed the occurrence of intermolecular electron transfer from triplet excited state of zinc porphyrins to CorTIm with diffusion-limited value in PhCN. Finally, the supramolecular interaction in cruciform pentamers contributes to the highly ordered patterning on the TEM grid. These findings provide a new perspective for the construction of efficient molecular electronic and light-energy conversion systems.

## Experimental Section

### Syntheses

**meso-10-Bromo zinc porphyrin (2):** Zinc porphyrin **1** (680 mg, 0.79 mmol) was dissolved in dichloromethane (57 mL) and pyridine

(0.96 mL), and the solution was cooled at 0 °C. Next, *N*-bromosuccinimide (140 mg, 0.79 mmol) was added to the solution, and it was stirred for 10 min. After adding acetone (10 mL) to the mixture, the solvent was evaporated. The product was purified over silica gel column using hexane/ethyl acetate (10:1 v/v) as eluent to afford porphyrin **2** as a red powder (647 mg (77%)). <sup>1</sup>H NMR (400 MHz, CDCl<sub>3</sub>): δ = 10.20 (s, 1H), 9.80 (d, *J* = 4.9 Hz, 2H), 9.34 (d, *J* = 4.9 Hz, 2H), 9.17 (d, *J* = 4.9 Hz, 2H), 9.16 (d, *J* = 4.9 Hz, 2H), 7.37 (d, *J* = 2.4 Hz, 4H), 6.90 (t, *J* = 2.4 Hz, 2H), 4.16 (t, *J* = 6.8 Hz, 8H), 1.89 (sept, *J* = 6.3 Hz, 4H), 1.77 (q, *J* = 6.8 Hz, 8H), 0.98 ppm (d, *J* = 6.3 Hz, 24H); <sup>13</sup>C NMR (100 MHz, CDCl<sub>3</sub>): δ = 158.25, 150.44, 150.30, 149.30, 143.98, 133.21, 133.07, 132.82, 132.04, 121.09, 114.41, 100.96, 66.76, 38.11, 25.13, 22.67 ppm; MALDI-TOF MS: *m/z* calcd for C<sub>52</sub>H<sub>59</sub>BrN<sub>4</sub>O<sub>4</sub>Zn: 946.30 [*M*+H]; found: 947.41; <sup>1</sup>H NMR spectrum is shown in Figure S8 (the Supporting Information).

**meso-10-(4-Phthalimidyl-phenyl)-zinc porphyrin (3):** Porphyrin **2** (480 mg, 0.51 mmol), 2-[4-(4,4,5,5-tetramethyl-1,3,2-dioxaborolan-2-yl)benzyl]isindoline-1,3-dione (180 mg, 0.51 mmol), Cs<sub>2</sub>CO<sub>3</sub> (250 mg, 0.76 mmol), and [Pd(PPh<sub>3</sub>)<sub>4</sub>] (58 mg, 0.051 mmol, 10 mol%) were dissolved in degassed toluene (64 mL) and DMF (32 mL). Then, the mixture solution was stirred at 80 °C for 10 h. After finishing the reaction, the mixture was extracted with toluene, and organic phase was dried over anhydrous Na<sub>2</sub>SO<sub>4</sub>. Then, the solvent was evaporated. The crude was purified over silica gel column using column chromatography (chloroform/hexane = 2:1) as eluent to afford porphyrin **3**. Red powder: 404 mg (72%), <sup>1</sup>H NMR (400 MHz, CDCl<sub>3</sub>): δ = 10.23 (s, 1H), 9.38 (d, *J* = 4.4 Hz, 2H), 9.19 (d, *J* = 4.4 Hz, 2H), 9.06 (d, *J* = 4.4 Hz, 2H), 8.91 (d, *J* = 4.4 Hz, 2H), 8.14 (d, *J* = 8.2 Hz, 2H), 7.94 (dd, *J* = 2.4, 2.4 Hz, 2H), 7.80–7.76 (m, 4H), 7.38 (d, *J* = 2.0 Hz, 4H), 6.88 (t, *J* = 2.0 Hz, 2H), 5.19 (s, 2H), 4.14 (t, *J* = 6.3 Hz, 8H), 1.88 (sept, *J* = 6.8 Hz, 4H), 1.76 (q, *J* = 6.8 Hz, 8H), 0.97 ppm (d, *J* = 6.8 Hz, 24H); <sup>13</sup>C NMR (100 MHz, CDCl<sub>3</sub>): δ = 158.19, 149.92, 149.83, 149.70, 144.50, 134.68, 133.97, 132.68, 131.85, 131.62, 126.59, 123.39, 114.39, 100.87, 66.72, 41.54, 38.12, 25.11, 22.65 ppm; MALDI-TOF MS: *m/z* calcd for C<sub>67</sub>H<sub>69</sub>N<sub>5</sub>O<sub>6</sub>Zn: 1103.45 [*M*+H]; found: 1104.40; <sup>1</sup>H NMR spectrum is shown in Figure S9 (the Supporting Information).

**meso-10-(4-Phthalimidyl-phenyl)-porphyrin (4):** Porphyrin **3** (350 mg, 0.32 mmol) was dissolved in CH<sub>2</sub>Cl<sub>2</sub>, and then TFA (35 mL) was added to the solution. The mixture solution was stirring at room temperature for 1 h. After diluting with water, organic phase was washed with saturated NaHCO<sub>3</sub> three times, and dried over Na<sub>2</sub>SO<sub>4</sub>. Then, the solvent was evaporated. The product was purified over silica gel column using chloroform as eluent to afford porphyrin **4**. Purple powder 320 mg (96%). <sup>1</sup>H NMR (400 MHz, CDCl<sub>3</sub>): δ = 10.19 (s, 1H), 9.32 (d, *J* = 4.4 Hz, 2H), 9.12 (d, *J* = 4.4 Hz, 2H), 8.98 (d, *J* = 4.4 Hz, 2H), 8.82 (d, *J* = 4.4 Hz, 2H), 8.15 (d, *J* = 4.4 Hz, 2H), 7.97 (dd, *J* = 2.9, 2.9 Hz, 2H), 7.81–7.78 (m, 4H), 7.38 (d, *J* = 2.4 Hz, 4H), 6.89 (t, *J* = 2.4 Hz, 2H), 5.21 (s, 2H), 4.16 (t, *J* = 6.8 Hz, 8H), 1.88 (sept, *J* = 6.8 Hz, 4H), 1.76 (q, *J* = 6.8 Hz, 8H), 0.97 (d, *J* = 6.8 Hz, 24H), –3.08 ppm (s, 2H); <sup>13</sup>C NMR (100 MHz, CDCl<sub>3</sub>): δ = 168.31, 158.40, 143.45, 142.13, 135.77, 134.76, 134.11, 132.24, 126.67, 123.52, 119.58, 114.43, 104.73, 100.98, 66.73, 41.53, 38.10, 25.10, 22.65 ppm; MALDI-TOF MS: *m/z* calcd for C<sub>52</sub>H<sub>61</sub>BrN<sub>4</sub>O<sub>4</sub>: 1041.54 [*M*+3H]; found: 1044.70; <sup>1</sup>H NMR spectrum is shown in Figure S10 (the Supporting Information).

**meso-10-(4-Aminomethyl-phenyl)-porphyrin (5):** Porphyrin **4** (320 mg) was dissolved in CH<sub>2</sub>Cl<sub>2</sub> (21 mL) and EtOH (21 mL). Hydrazine monohydrate (4.3 mL) was added to the solution and heated at reflux for 5 h. After cooling to room temperature, the mixture was extracted with CH<sub>2</sub>Cl<sub>2</sub>, and the organic phase was dried over anhydrous Na<sub>2</sub>SO<sub>4</sub>. Then, by evaporating the solvent, porphyrin **5** was obtained. Purple powder 270 mg (96%). <sup>1</sup>H NMR (400 MHz,

CDCl<sub>3</sub>):  $\delta$  = 10.20 (s, 1H), 9.32 (d,  $J$  = 4.4 Hz, 2H), 9.13 (d,  $J$  = 4.4 Hz, 2H), 9.01 (d,  $J$  = 4.4 Hz, 2H), 8.86 (d,  $J$  = 4.4 Hz, 2H), 8.17 (d,  $J$  = 7.4 Hz, 2H), 7.69 (d,  $J$  = 7.4 Hz, 2H), 7.40 (d,  $J$  = 2.0 Hz, 4H), 6.90 (t,  $J$  = 2.0 Hz, 2H), 4.25 (s, 2H), 4.16 (t,  $J$  = 6.8 Hz, 8H), 4.14 (brs, 2H) 1.88 (sept,  $J$  = 6.4 Hz, 4H), 1.77 (q,  $J$  = 6.8 Hz, 8H), 0.98 (d,  $J$  = 6.4 Hz, 24H), -3.05 ppm (s, 2H); <sup>13</sup>C NMR (100 MHz, CDCl<sub>3</sub>):  $\delta$  = 158.44, 143.51, 142.62, 141.03, 134.64, 125.25, 120.34, 119.51, 114.47, 104.67, 101.00, 66.74, 46.46, 38.12, 25.11, 22.65 ppm; MALDI-TOF MS:  $m/z$  calcd for C<sub>59</sub>H<sub>69</sub>N<sub>5</sub>O<sub>4</sub>: 911.53 [ $M+2H$ ]; found: 913.06. The <sup>1</sup>H NMR spectrum is shown in Figure S11 (the Supporting Information).

**(H<sub>2</sub>P)<sub>4</sub>-CorTIm:** CorDIm(*i*Bu)<sub>4</sub> (120 mg, 0.13 mmol) and KOH (1.5 g, 27 mmol) were added to *n*-BuOH (15 mL), and the solution was stirred at 120 °C for 10 h. After cooling to room temperature, H<sub>2</sub>O (20 mL) was added to the mixture solution. Then, after adding excess volume of AcOH to the solution, it was stirred at room temperature for 3 h. After the reaction was complete, the resulting solid was collected by filtration. The solid was washed in water several times. The solid was dried in vacuo for 4 h. Next, obtained solid (24 mg) and porphyrin **5** (200 mg) were dissolved in DMF (15 mL) and stirred at 150 °C for 12 h. After cooling to room temperature, the solvent was evaporated. The crude was purified over silica gel column using CHCl<sub>3</sub>. Finally, the product was purified by size exclusion chromatography using toluene. Red purple solid: 5.0 mg (1.0%); <sup>1</sup>H NMR (400 MHz, CDCl<sub>3</sub>):  $\delta$  = 10.08 (brs, 1H), 10.00 (brs, 1H), 9.15 (brd, 4H), 8.91 (brd, 4H), 8.64 (brd, 2H), 8.4 (brd, 6H), 7.10 (brs, 2H), 5.30 (brs, 2H), 3.80 (brs, 8H), 1.92 (brs, 4H), 1.77 (brs, 8H), 0.64 (brd, 24H), -3.16 ppm (brs, 2H); <sup>13</sup>C NMR (100 MHz, CDCl<sub>3</sub>):  $\delta$  = 167.77, 159.38, 158.14, 157.76, 143.25, 135.21, 134.96, 134.80, 131.31, 130.90, 129.67, 128.95, 128.04, 125.66, 125.39, 125.02, 119.61, 119.34, 118.74, 114.21, 104.66, 100.71, 66.41, 37.86, 37.66, 24.85, 23.91, 22.45 ppm; MALDI-TOF MS:  $m/z$  calcd for C<sub>258</sub>H<sub>252</sub>N<sub>20</sub>O<sub>22</sub>: 4154.07 [ $M-4H$ ]; found: 4150.10; <sup>1</sup>H NMR and MALDI-TOF mass spectra are shown in Figure S1 (the Supporting Information).

**(ZnP)<sub>4</sub>-CorTIm:** CorDIm(*i*Bu)<sub>4</sub> (4.0 mg, 0.13 mmol) and [Zn(OAc)<sub>2</sub>] (0.98 g, 5.4 mmol) were dissolved in CH<sub>2</sub>Cl<sub>2</sub> (4.0 mL) and MeOH (0.40 mL). Then, the solution was stirred at 50 °C for 1 h. After diluting with water, organic phase was washed with saturated NaHCO<sub>3</sub> three times, and dried over Na<sub>2</sub>SO<sub>4</sub>. Then, the solvent was evaporated. The crude was purified over silica gel column using CHCl<sub>3</sub>. Finally, the product was purified by size exclusion chromatography using toluene. Red purple solid: 4.0 mg (94%); <sup>1</sup>H NMR (400 MHz, CDCl<sub>3</sub>):  $\delta$  = 10.13 (brs, 1H), 10.06 (brs, 1H), 9.23 (brd, 4H), 8.97 (brd, 4H), 8.70 (brd, 2H), 8.46 (brd, 6H), 7.00 (brs, 2H), 6.50 (brs, 2H), 3.11 (brs, 8H), 1.94 (brs, 12H), 0.79 ppm (brd, 24H); MALDI-TOF MS:  $m/z$  calcd for C<sub>258</sub>H<sub>244</sub>N<sub>20</sub>O<sub>22</sub>Zn<sub>4</sub>: 4401.72 [ $M$ ]; found: 4401.70.

## Acknowledgements

This work was partially supported by Grants-in-Aid for Scientific Research (Nos. 26286017, 26620159, 15H01003, 15H01094 to T.H., Nos. 26620154&26288037 to K.O., No. 25886012 to H.S.), an Advanced Low Carbon Technology Research and Development (ALCA) program from Japan Science Technology Agency (JST to S.F.) and the Science Research Promotion Fund from the Promotion and Mutual Aid Corporation for Private Schools from MEXT, Japan, and Mitsubishi Foundation.

**Keywords:** dyes/pigments • electron transfer • energy transfer • porphyrins • zinc

- [1] a) M. D. Watson, A. Fechtenkotter, K. Müllen, *Chem. Rev.* **2001**, *101*, 1267–1300; b) J. Wu, W. Pisula, K. Müllen, *Chem. Rev.* **2007**, *107*, 718–747; c) T. Aida, E. W. Meijer, S. I. Stupp, *Science* **2012**, *335*, 813–817; d) R. J. Bushby, O. R. Lozman, *Curr. Opin. Colloid Interface Sci.* **2002**, *7*, 343–354; e) S. Laschat, A. Baro, N. Steinke, F. Giesselmann, C. Hägele, G. Scalia, R. Judele, E. Kapatsina, S. Sauer, A. Schreivogel, M. Tosoni, *Angew. Chem. Int. Ed.* **2007**, *46*, 4832–4887; *Angew. Chem.* **2007**, *119*, 4916–4973; f) S. Kumar, *Chem. Soc. Rev.* **2006**, *35*, 83–109.
- [2] a) V. M. Blas-Ferrando, J. Ortiz, K. Ohkubo, S. Fukuzumi, F. Fernandez-Lazaro, Á. Sastre-Santos, *Chem. Sci.* **2014**, *5*, 4785–4793; b) F. J. Céspedes-Guirao, K. Ohkubo, S. Fukuzumi, Á. Sastre-Santos, F. Fernández-Lázaro, *J. Org. Chem.* **2009**, *74*, 5871–5880; c) S. Fukuzumi, K. Ohkubo, J. Ortiz, A. M. Gutierrez, F. Fernandez-Lazaro, Á. Sastre-Santos, *Chem. Commun.* **2005**, 3814–3816; d) V. M. Blas-Ferrando, J. Ortiz, L. Bouissane, K. Ohkubo, S. Fukuzumi, F. Fernandez-Lazaro, Á. Sastre-Santos, *Chem. Commun.* **2012**, *48*, 6241–6243; e) S. Fukuzumi, K. Ohkubo, J. Ortiz, A. M. Gutiérrez, F. Fernández-Lázaro, Á. Sastre-Santos, *J. Phys. Chem. A* **2008**, *112*, 10744–10752; f) M. E. El-Khouly, M. Jaggi, B. Schmid, C. Blum, S.-X. Liu, S. Decurtins, K. Ohkubo, S. Fukuzumi, *J. Phys. Chem. C* **2011**, *115*, 8325–8334; g) Á. J. Jiménez, F. Spänig, M. S. Rodríguez-Morgade, K. Ohkubo, S. Fukuzumi, D. M. Guldi, T. Torres, *Org. Lett.* **2007**, *9*, 2481–2484; h) M. R. Wasielewski, *Acc. Chem. Res.* **2009**, *42*, 1910–1921; i) T. M. Wilson, M. J. Tauber, M. R. Wasielewski, *J. Am. Chem. Soc.* **2009**, *131*, 8952–8957; j) R. K. Dubey, M. Niemi, K. Kaunisto, K. Stranius, A. Efimov, N. V. Tkachenko, H. Lemmetyinen, *Inorg. Chem.* **2013**, *52*, 9761–9773; k) R. Gómez, D. Veldman, R. Blanco, C. Seoane, J. L. Segura, R. A. J. Janssen, *Macromolecules* **2007**, *40*, 2760–2772; l) S. J. Kang, S. Ahn, J. B. Kim, C. Schenck, A. M. Hiszpanski, S. Oh, T. Schiros, Y.-L. Loo, C. Nuckolls, *J. Am. Chem. Soc.* **2013**, *135*, 2207–2212.
- [3] a) H.-Y. Chen, C.-T. Chen, C.-T. Chen, *Macromolecules* **2010**, *43*, 3613–3623; b) K. Sawabe, M. Imakawa, M. Nakano, T. Yamao, S. Hotta, Y. Iwasa, T. Takenobu, *Adv. Mater.* **2012**, *24*, 6141–6146; c) U. Rohr, P. Schlichting, A. Bohm, M. Gross, K. Meerholz, C. Bräuchle, K. Müllen, *Angew. Chem. Int. Ed.* **1998**, *37*, 1434–1437; *Angew. Chem.* **1998**, *110*, 1463–1467; d) B. Zhao, B. Liu, R. Q. Png, K. Zhang, K. A. Lim, J. Luo, J. Shao, P. K. H. Ho, C. Chi, J. Wu, *Chem. Mater.* **2010**, *22*, 435–449.
- [4] a) L. Schmidt-Mende, A. Fechtenkötter, K. Müllen, E. Moons, R. H. Friend, J. D. MacKenzie, *Science* **2001**, *293*, 1119–1122; b) J. L. Li, M. Kastler, W. Pisula, J. W. F. Robertson, D. Wasserfallen, A. C. Grimsdale, J. S. Wu, K. Müllen, *Adv. Funct. Mater.* **2007**, *17*, 2528–2533; c) Y. Yamamoto, G. Zhang, W. Jina, T. Fukushima, N. Ishii, A. Saeki, S. Sekie, S. Tagawa, T. Minari, K. Tsukagoshi, T. Aida, *Proc. Natl. Acad. Sci. USA* **2009**, *106*, 21051–21056.
- [5] a) S. Hirayama, H. Sakai, Y. Araki, M. Tanaka, M. Imakawa, T. Wada, T. Takenobu, T. Hasobe, *Chem. Eur. J.* **2014**, *20*, 9081–9093; b) A. Dadvand, A. G. Moiseev, K. Sawabe, W.-H. Sun, B. Djukic, I. Chung, T. Takenobu, F. Rosei, D. F. Perepichka, *Angew. Chem. Int. Ed.* **2012**, *51*, 3837–3841; *Angew. Chem.* **2012**, *124*, 3903–3907; c) J. E. Anthony, *Angew. Chem. Int. Ed.* **2008**, *47*, 452–483; *Angew. Chem.* **2008**, *120*, 460–492; d) O. D. Jurchescu, M. Popinciuc, B. J. van Wees, T. T. M. Palstra, *Adv. Mater.* **2007**, *19*, 688–692; e) S. Pola, C.-H. Kuo, W.-T. Peng, M. M. Islam, I. Chao, Y.-T. Tao, *Chem. Mater.* **2012**, *24*, 2566–2571; f) B. Yoo, T. Jung, D. Basu, A. Dodabalapur, B. A. Jones, A. Facchetti, M. R. Wasielewski, T. J. Marks, *Appl. Phys. Lett.* **2006**, *88*, 082104; g) S. Xiao, M. Myers, Q. Miao, S. Sanaur, K. Pang, M. L. Steigerwald, C. Nuckolls, *Angew. Chem. Int. Ed.* **2005**, *44*, 7390–7394; *Angew. Chem.* **2005**, *117*, 7556–7560; h) M. Más-Montoya, R. P. Ortiz, D. Curiel, A. Espinosa, M. Allain, A. Facchetti, T. J. Marks, *J. Mater. Chem. C* **2013**, *1*, 1959–1969.
- [6] a) S. Fukuzumi, K. Ohkubo, T. Suenobu, *Acc. Chem. Res.* **2014**, *47*, 1455–1464; b) S. Fukuzumi, *Bull. Chem. Soc. Jpn.* **2006**, *79*, 177–195; c) D. Gust, T. A. Moore, A. L. Moore, *Acc. Chem. Res.* **2009**, *42*, 1890–1898; d) D. Gust, T. A. Moore, A. L. Moore, *Acc. Chem. Res.* **2001**, *34*, 40–48; e) S. Kirner, M. Sekita, D. M. Guldi, *Adv. Mater.* **2014**, *26*, 1482–1493; f) T. Umeyama, H. Imahori, *J. Phys. Chem. C* **2013**, *117*, 3195–3209; g) F. D'Souza, O. Ito, *Chem. Soc. Rev.* **2012**, *41*, 86–96.

- [7] a) S. M. M. Conron, L. E. Shoer, A. L. Smeigh, A. B. Ricks, M. R. Wasielewski, *J. Phys. Chem. B* **2013**, *117*, 2195–2204; b) F. Würthner, *Chem. Commun.* **2004**, 1564–1579; c) A. P. H. J. Schenning, J. v. Herrikhuyzen, P. Jonkheijm, Z. Chen, F. Würthner, E. W. Meijer, *J. Am. Chem. Soc.* **2002**, *124*, 10252–10253; d) L. Flamigni, A. I. Ciuciu, H. Langhals, B. Böck, D. T. Gryko, *Chem. Asian J.* **2012**, *7*, 582–592.
- [8] a) R. Dabirian, V. Palermo, A. Liscio, E. Schwartz, M. B. J. Otten, C. E. Finlayson, E. Treossi, R. H. Friend, G. Calestani, K. Müllen, R. J. M. Nolte, A. E. Rowan, P. Samori, *J. Am. Chem. Soc.* **2009**, *131*, 7055–7063; b) K. M. Lefler, C. H. Kim, Y.-L. Wu, M. R. Wasielewski, *J. Phys. Chem. Lett.* **2014**, *5*, 1608–1615; c) D. Khim, K.-J. Baeg, J. Kim, M. Kang, S.-H. Lee, Z. Chen, A. Facchetti, D.-Y. Kim, Y.-Y. Noh, *ACS Appl. Mater. Interfaces* **2013**, *5*, 10745–10752; d) N. Karousis, J. Ortiz, K. Ohkubo, T. Hasobe, S. Fukuzumi, Á. Sastre-Santos, N. Tagmatarchis, *J. Phys. Chem. C* **2012**, *116*, 20564–20573.
- [9] a) S. Alibert-Fouet, I. Seguy, J.-F. Bobo, P. Destruel, H. Bock, *Chem. Eur. J.* **2007**, *13*, 1746–1753; b) Y. Avlasevich, S. Müller, P. Erk, K. Müllen, *Chem. Eur. J.* **2007**, *13*, 6555–6561; c) C. D. Schmidt, N. Lang, N. Jux, A. Hirsch, *Chem. Eur. J.* **2011**, *17*, 5289–5299; d) K. Ida, H. Sakai, K. Ohkubo, Y. Araki, T. Wada, T. Sakanoue, T. Takenobu, S. Fukuzumi, T. Hasobe, *J. Phys. Chem. C* **2014**, *118*, 7710–7720.
- [10] S. Fukuzumi, K. Ohkubo, *J. Mater. Chem.* **2012**, *22*, 4575–4587.
- [11] a) A. Satake, Y. Kobuke, *Tetrahedron* **2005**, *61*, 13–41; b) M. Beyler, L. Flamigni, V. Heitz, J.-P. Sauvage, B. Ventura, *Photochem. Photobiol.* **2014**, *90*, 275–286; c) V. K. Praveen, C. Ranjith, E. Bandini, A. Ajayaghosh, N. Armaroli, *Chem. Soc. Rev.* **2014**, *43*, 4222–4242; d) J. Yang, M.-C. Yoon, H. Yoo, P. Kim, D. Kim, *Chem. Soc. Rev.* **2012**, *41*, 4808–4826.
- [12] K. Ohkubo, H. Kotani, J. Shao, Z. Ou, K. M. Kadish, G. Li, R. K. Pandey, M. Fujitsuka, O. Ito, H. Imahori, S. Fukuzumi, *Angew. Chem. Int. Ed.* **2004**, *43*, 853–856; *Angew. Chem.* **2004**, *116*, 871–874.
- [13] a) T. Hasobe, M. G. Rabbani, A. S. D. Sandanayaka, H. Sakai, T. Murakami, *Chem. Commun.* **2010**, 46, 889–891; b) T. Hasobe, *J. Phys. Chem. Lett.* **2013**, *4*, 1771–1780; c) T. Hasobe, *Phys. Chem. Chem. Phys.* **2010**, *12*, 44–57; d) M. U. Winters, E. Dahlstedt, H. E. Blades, C. J. Wilson, M. J. Frampton, H. L. Anderson, B. Albinsson, *J. Am. Chem. Soc.* **2007**, *129*, 4291–4297; e) N. Aratani, D. Kim, A. Osuka, *Acc. Chem. Res.* **2009**, *42*, 1922–1934; f) S. Kuhri, V. Engelhardt, R. Faust, D. M. Guldi, *Chem. Sci.* **2014**, *5*, 2580–2588; g) S. Fukuzumi, K. Saito, K. Ohkubo, V. Troiani, H. Qiu, S. Gadde, F. D'Souza, N. Solladie, *Phys. Chem. Chem. Phys.* **2011**, *13*, 17019–17022.
- [14] a) W.-S. Li, T. Aida, *Chem. Rev.* **2009**, *109*, 6047–6076; b) J. Yang, S. Cho, H. Yoo, J. Park, W.-S. Li, T. Aida, D. Kim, *J. Phys. Chem. A* **2008**, *112*, 6869–6876; c) S. Fukuzumi, K. Saito, K. Ohkubo, T. Khoury, Y. Kashiwagi, M. A. Absalom, S. Gadde, F. D'Souza, Y. Araki, O. Ito, M. J. Crossley, *Chem. Commun.* **2011**, 47, 7980–7982; d) T. Hasobe, Y. Kashiwagi, M. A. Absalom, J. Sly, K. Hosomizu, M. J. Crossley, H. Imahori, P. V. Kamat, S. Fukuzumi, *Adv. Mater.* **2004**, *16*, 975–979; e) J. Larsen, J. Andersson, T. Polivka, J. Sly, M. J. Crossley, V. Sundstrom, E. Akesson, *Chem. Phys. Lett.* **2005**, *403*, 205–210; f) Y.-H. Jeong, M. Son, H. Yoon, P. Kim, D.-H. Lee, D. Kim, W.-D. Jang, *Angew. Chem. Int. Ed.* **2014**, *53*, 6925–6928.
- [15] Z. Gasyna, W. R. Browett, M. J. Stillman, *Inorg. Chem.* **1985**, *24*, 2440–2447.
- [16] a) L. R. Nudy, H. G. Hutchinson, C. Schieber, F. R. Longo, *Tetrahedron* **1984**, *40*, 2359–2363; b) A. G. Hyslop, M. A. Kellett, P. M. Iovine, M. J. Therien, *J. Am. Chem. Soc.* **1998**, *120*, 12676–12677.
- [17] N. Aratani, A. Osuka, *Org. Lett.* **2001**, *3*, 4213–4216.
- [18] Y. Kawashima, K. Ohkubo, S. Fukuzumi, *J. Phys. Chem. A* **2012**, *116*, 8942–8948.
- [19] Many examples concerning the similar blueshifted trends of radical anion species were reported in the case of covalently linked donor-acceptor systems containing fullerene derivatives because of electronic interactions in the oxidized and/or reduced states. See Ref. [6].
- [20] a) R. van Hameren, P. Schon, A. M. van Buul, J. Hoogboom, S. V. Lazarenko, J. W. Gerritsen, H. Engelkamp, P. C. M. Christianen, H. A. Heus, J. C. Maan, T. Rasing, S. Speller, A. E. Rowan, J. A. A. W. Elemans, R. J. M. Nolte, *Science* **2006**, *314*, 1433–1436; b) T. Aoki, H. Sakai, K. Ohkubo, T. Sakanoue, T. Takenobu, S. Fukuzumi, T. Hasobe, *Chem. Sci.* **2015**, *6*, 1498–1509.
- [21] Z. An, J. Yu, B. Domercq, S. C. Jones, S. Barlow, B. Kippelen, S. R. Marder, *J. Mater. Chem.* **2009**, *19*, 6688–6698.

Received: February 25, 2015

Published online on June 19, 2015